Electric dipole spin resonance at shallow donors in quantum wires

D. V. Khomitsky,[1,*] E. A. Lavrukhina,[1] and E. Ya. Sherman[2,3]

[1]*Department of Physics, National Research Lobachevsky State University of Nizhni Novgorod, 603950 Gagarin Avenue 23, Nizhny Novgorod, Russian Federation*

[2]*Department of Physical Chemistry, The University of the Basque Country, 48080 Bilbao, Spain*

[3]*IKERBASQUE, Basque Foundation for Science, Bilbao, Spain*

(Received 8 July 2018; revised manuscript received 7 December 2018; published 30 January 2019)

Electric dipole spin resonance is studied theoretically for a shallow donor formed in a nanowire with spin-orbit coupling in a magnetic field. Such a system may represent a donor-based qubit. The single discrete energy level of the donor is accompanied by a set of continuum states, which provide a nontrivial interplay for the picture of electric dipole spin resonance driven by an external monochromatic field. Strongly nonlinear dependencies of spin-flip time as well as of the coordinate mean values on the electric field amplitude are observed, demonstrating the significance of coupling to the continuum for spin-based qubit manipulation in nanostructures.

DOI: 10.1103/PhysRevB.99.014308

I. INTRODUCTION

Electric dipole spin resonance (EDSR), i.e., the ability to manipulate spins of charge carriers by an electric rather than a magnetic field, is one of the most distinctive features of spin-orbit coupling (SOC). It was predicted theoretically [1] and initially observed experimentally for itinerant electrons in bulk crystals [2–4], soon after which it was studied theoretically in detail for electrons localized on donors [5] and for holes on the acceptor centers [6]. More recently, it was shown that EDSR is a powerful tool for spin manipulation in quantum wells [7] and other two-dimensional heterostructures with spin-orbit coupling [8]. In addition, EDSR can be used to manipulate electric current in low-dimensional conductors [9]. The observation of EDSR in quantum dots [10] paved the way for their applications in spin-based quantum computing, where the spin of a carrier localized in a quantum dot is considered to be a qubit. Single electron spin manipulation using hybrid semiconductor-superconductor systems has been proposed in Ref. [11]. As a result, theoretical studies of EDSR in quantum dots attracted a great deal of interest among researchers [12–14]. The importance of several effects, including nonlinear dynamics, has been recognized and investigated [15,16]. Spin manipulation by pulsed rather than periodic electric fields has been studied, e.g., in Ref. [17] for designed pulses and in Ref. [18] for subcycle ones. Also, EDSR can occur in quantum wires [19], making it of great interest [20] in the field of information-processing technology. Another interesting example of EDSR can be found in carbon nanotubes [21].

Recently, other kinds of solid-state-based qubits have been put forward. These states are related to the Majorana fermions [22–26] in InSb-based nanowires, demonstrating rich disorder effects on the electron states [27]. Another option is related to using shallow electron states as qubits [28]. Here studies of EDSR face a challenge, which has not yet been addressed in the literature, because in shallow donor systems the applied electric field can couple the localized and delocalized states of the electron. Also, such a modification of the states could be produced by spin-orbit coupling. As a result, the electron wave functions, spin-flip transition matrix elements, and the entire spin dynamics become strongly modified. Shallow states in nanowires can be formed by charged donors screened by itinerant electrons in the surrounding metallic gates or in the two-dimensional electron gas used as a building element of the template structure.

Note that the above-mentioned approaches considered either itinerant or localized states without taking into account possible transitions to continuum states, as can occur for shallow donors. Here we address these issues and show how the entire picture of EDSR for shallow states is modified in the presence of the continuum.

This paper is organized as follows. In Sec. II we introduce the model of single-electron states formed in a nanowire in the presence of a shallow donor potential, the SOC, and the magnetic field. Both localized and delocalized states are considered, and the periodic potential of the driving electric field is introduced. In Sec. III we present the results of the perturbation theory approach, which allows us to highlight several key features of the quantum states, including those stemming from the interplay of SOC and the magnetic field. In Sec. IV the numerical solution for the time-dependent problem with the driving is discussed, and the main results of the paper are presented for various parameters of the model. In Sec. V we give our conclusions.

II. MODEL HAMILTONIAN AND EXTERNAL DRIVING

We consider a narrow nanowire, elongated along the x-axis, as shown in Fig. 1(a), where the full three-dimensional (3D) electron wave function $\psi_{3D}(\mathbf{r})$ can be presented as a product $\psi_{3D}(\mathbf{r}) = \psi_{2D}(\mathbf{r}_\perp)\Psi(x,t)$. Here $\psi_{2D}(\mathbf{r}_\perp)$ corresponds to the ground state of the transverse motion with

*khomitsky@phys.unn.ru

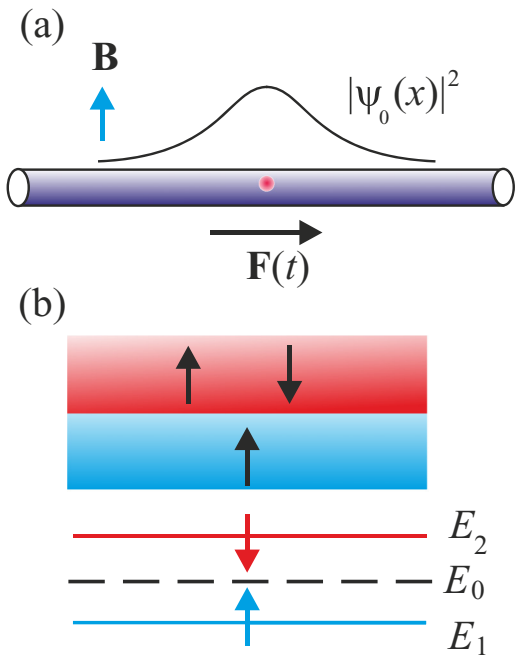

FIG. 1. (a) A schematic layout of a shallow donor (shown by closed circle) state formed in a quantum wire. The vectors **B** and **F**(t) show the directions of an applied constant magnetic field and a periodic electric field, respectively. (b) Scheme of the Zeeman doublet E_1, E_2 and the continuum states shown in the shaded bands. Arrows correspond to orientation of spins.

$\mathbf{r}_\perp = (y, z)$, and we will be interested only in the motion along the wire described by $\Psi(x, t)$.

To characterize this one-dimensional motion, we begin with the following Hamiltonian using the effective-mass approximation:

$$H_0 = \frac{p^2}{2m} - \frac{U_0}{\cosh^2(x/d)}, \tag{1}$$

where the confinement by the donor is described as a potential with the effective width d and the maximum depth U_0, m is the electron effective mass, and $p = -i\hbar\partial/\partial x \equiv \hbar k$ is the momentum operator. We are interested here in shallow potentials satisfying the condition of weak binding, such as $\hbar^2/md^2 \gg U_0$. In general, in such potentials the binding energy E_0 is determined by $E_0 \sim -m(U_0 d)^2/\hbar^2$. Omitting for the moment the spinor structure, we present the ground-state wave function at distances $|x| \gg d$ in the form [29]

$$\psi_0(x) = \frac{1}{\sqrt{l}} \exp(-|x|/l), \tag{2}$$

with the localization length $l = \sqrt{\hbar^2/2m|E_0|} \gg d$.

Next, we add the Rashba SOC $H_R = \alpha\sigma_y k$ and the constant magnetic field $\mathbf{B} = (0, 0, B)$ (see Fig. 1) creating the Zeeman term in the Hamiltonian, which now takes the following form:

$$H_1 = H_0 + \frac{\Delta}{2}\sigma_z + \alpha\sigma_y k. \tag{3}$$

Here the Zeeman splitting $\Delta = \mu_B g B$, where μ_B is the Bohr magneton and g is the electron g-factor. Since we consider a narrow single quantum wire in the ground-state transverse mode, we employ the basic form of the Rashba coupling. A description of the Rashba coupling in more complex nanowire systems can be found, e.g., in Refs. [30–33].

As a result, the ground state of (1) transforms into a Zeeman-split doublet containing the only two localized eigenstates of (3), with spacing $E_2 - E_1$ [see Fig. 1(b)]. For $\alpha = 0$ and $g < 0$, the ground state E_1 is the spin-up state where the spin is parallel to the magnetic field, and the state E_2 is the spin-down state. These Zeeman partners may effectively participate in the spin resonance driven by an external periodic electric field applied along the wire, with frequency $\omega = (E_2 - E_1)/\hbar$ and amplitude F_0, and described as a potential,

$$V(x, t) = eF_0 x \sin\omega t, \tag{4}$$

where e is the fundamental charge, being added to the Hamiltonian H_1. The reason for this participation is that due to the presence of SOC, the eigenstates of (3) contain both spinor components. Therefore, two states with different signs of their σ_z can still be coupled by the electric field potential described in (4) by the position operator, creating the possibility of electric dipole spin resonance.

As for the continuum states, they also split into Zeeman doublets, as shown in Fig. 1(b) by arrows in the bands above E_1 and E_2. At $\alpha = 0$ and $g < 0$, the low-energy part of the continuum has spin-up and is nondegenerate. The higher states are twofold-degenerate, where the spin-up state from the lower Zeeman energy is accompanied by the spin-down state from the higher Zeeman energy described by the eigenvalue set of continuum for H_0.

In the absence of spin-orbit coupling, with the increase in the magnetic field, the discrete state E_2 reaches the bottom of the continuum at the merging field B_m satisfying the condition

$$\mu_B |g| B_m = |E_0|, \tag{5}$$

and transition frequency $\omega = |E_0| \times (B/B_m)/\hbar$. Below we will consider fields lower than B_m in order to avoid the direct overlap of the discrete and continuum states in the stationary Hamiltonian (3). However, we will see that discrete and continuum states interact dynamically during the evolution driven by a periodic electric field, as will be discussed in the next sections.

III. SPIN-ORBIT COUPLING AS A PERTURBATION

For a qualitative understanding of electric dipole spin resonance, here we will apply the perturbation theory to highlight the effects of SOC and the presence of continuum on the wave functions belonging only to the lowest Zeeman-split doublet. We begin by considering the SOC term $\alpha\sigma_y k$ in the Hamiltonian (3) as a perturbation, similar to the approaches of Refs. [5,34]. At $\alpha = 0$, we label the Zeeman-split doublet states as a spin-up ($\lambda = 1$) or a spin-down ($\lambda = -1$), respectively.

The states of the discrete spectrum have the form

$$\psi_0^{\lambda=-1} = \begin{bmatrix} 0 \\ \psi_0(x) \end{bmatrix}, \quad \psi_0^{\lambda=1} = \begin{bmatrix} \psi_0(x) \\ 0 \end{bmatrix}. \tag{6}$$

The energies of this Zeeman doublet are $E_0^{[\lambda]} = E_0 + \lambda\Delta/2$, and the only shallow localized ground state is $\psi_0(x)$. At $\alpha = 0$, $E_0^{\lambda=1} = E_1$ and $E_0^{\lambda=-1} = E_2$.

The continuum states are modeled by the approximation of extremely far hard walls located at $|x| = L$ with $L \gg l$, corresponding to the wire length $2L$, which leads to the set of very densely located levels representing the continuum with required accuracy [35]. The spatially odd states representing the continuous spectrum and coupled by the k term to the even localized states are labeled by the discrete index n in our model:

$$\varphi_n^{\lambda=-1} = \begin{bmatrix} 0 \\ \varphi_n(x) \end{bmatrix}, \qquad \varphi_n^{\lambda=1} = \begin{bmatrix} \varphi_n(x) \\ 0 \end{bmatrix}, \tag{7}$$

with the above defined energies $E_n^{[\lambda]} = E_n + \lambda\Delta/2$ and

$$\varphi_n(x) = \frac{1}{\sqrt{L}} \sin(k_n x), \tag{8}$$

where $E_n = \hbar^2 k_n^2/2m$ with $k_n = \pi n/L$.

When the SOC is turned on, the localized states (6) forming the ground Zeeman doublet acquire the admixture from the continuum states. In the leading order of the perturbation theory, one can present them as

$$\psi^{\lambda=-1} = \begin{bmatrix} \sum_n a_n^{\lambda=-1}\varphi_n(x) \\ \psi_0(x) \end{bmatrix}, \quad \psi^{\lambda=1} = \begin{bmatrix} \psi_0(x) \\ \sum_n a_n^{\lambda=1}\varphi_n(x) \end{bmatrix}, \tag{9}$$

where

$$a_n^{[\lambda]} = -\lambda \frac{\alpha}{E_0^{[\lambda]} - E_n^{[\lambda']}} \int_{-\infty}^{\infty} \varphi_n(x)\psi_0'(x)dx, \tag{10}$$

and for the wave function in Eq. (2) one obtains

$$\int_{-\infty}^{\infty} \varphi_n(x)\psi_0'(x)dx = -\frac{2}{\sqrt{lL}} \frac{k_n l}{1 + k_n^2 l^2}. \tag{11}$$

By analyzing (10) and (11), one can see that the coefficients $a_n^{[\lambda]}$ describing the admixture of continuum states for the localized Zeeman-split doublet (9) are proportional to α. This is a simple confirmation of the role played by the continuum states when the SOC is significant. The resulting spin-projected probability to find the electron in the continuum, $w_c = \sum_n |a_n^{[\lambda]}|^2$, at $B = 0$ is given by $w_c = m(\alpha/\hbar)^2/|E_0|$.

For the following studies of electric dipole spin resonance, we will need the matrix element of the coordinate calculated between the states of our interest, that is, between $\psi^{\lambda=1}$ and $\psi^{\lambda=-1}$ in Eq. (9). For the localized states (9) with opposite spins, one obtains

$$x_{\lambda\lambda'} = \sum_n \left(a_n^{\lambda=-1} + a_n^{\lambda=1}\right) \int_{-\infty}^{\infty} \varphi_n(x) x \psi_0(x) dx. \tag{12}$$

Taking into account that

$$\int_{-\infty}^{\infty} \varphi_n(x) x \psi_0(x) dx = 4\sqrt{\frac{l}{L}} l \frac{k_n l}{\left(1 + k_n^2 l^2\right)^2}, \tag{13}$$

performing summation over k_n, and by using (2),(8) and (10),(11), we arrive at

$$x_{\lambda\lambda'} = \frac{\alpha}{|E_0|} \frac{1}{\xi^3} [\xi^2 + 4(\sqrt{1-\xi} + \sqrt{1+\xi} - 2)], \tag{14}$$

with notation $\xi \equiv \Delta/|E_0| = B/B_m$. We consider $|\xi| < 1$ to avoid direct overlap of the continuum and localized states, where the energy levels acquire more complicated contributions. By expanding Eq. (14) by $\xi \ll 1$, we obtain $x_{\lambda\lambda'} = -5\alpha\xi/16|E_0|$. Note that the matrix element in Eq. (14) can be estimated in terms of two characteristic lengths of the model as $l \times l/l_{so}$, with $l_{so} = \hbar^2/m\alpha$ being the spin precession length. While this is the result of the first-order perturbation theory, which may no longer be applicable for large SOC, it clearly shows the importance of considering the continuum states for the system with a shallow donor and strong SOC. Thus, the Zeeman-split discrete states are SOC-coupled via the continuum. This coupling is critical for the driven dynamics, which will be analyzed in the next section.

In a similar way, we calculate the energy shift of the state of interest as

$$\Delta E^{[\lambda]} = -2m \frac{\alpha^2}{\hbar^2 \xi^2} (\sqrt{1 - \lambda\xi} - 1)^2. \tag{15}$$

In the zero-field limit $\xi \to 0$ both $\Delta E^{\lambda=-1}$ and $\Delta E^{\lambda=1}$ behave as $-m(\alpha/\hbar)^2/2$ and their difference $\Delta E^{\lambda=-1} - \Delta E^{\lambda=1} \approx m(\alpha/\hbar)^2\xi/2$. These corrections can be considered as a renormalization of the g-factor by the spin-orbit coupling due to the presence of the continuum states, and they show that the perturbation theory is applicable at $m(\alpha/\hbar)^2/|E_0| \ll 1$, that is, at $l \ll l_{so}$ and $|x_{\lambda\lambda'}| \ll l$.

IV. SPIN DYNAMICS FOR PERIODIC DRIVING

A. Numerical basis states and model of the dynamics

The numerically precise basis states ϕ_n and the energies $E_n^{(0)}$ of the Hamiltonian (1) are found by discretization on the x-axis. An eigenstate $\psi_s(x)$, where index s numerates the states, for (3) with the eigenenergy E_l is constructed as a superposition of the basis states ϕ_n of the Hamiltonian (1) with the coefficients forming two-component spinors:

$$\psi_s(x) = \sum_n \begin{bmatrix} a_n^s \\ b_n^s \end{bmatrix} \phi_n(x). \tag{16}$$

The spinor coefficients a_n^s and b_n^s are found from the numerical diagonalization of (3) with $s = 1, \ldots, s_{max}$, where s_{max} is the basis size.

Then, we solve numerically the nonstationary Schrödinger equation

$$i\hbar \frac{\partial}{\partial t} \Psi(x,t) = H(x,t)\Psi(x,t), \tag{17}$$

with the Hamiltonian $H(x,t) = H_1 + V(x,t)$, for the time-dependent wave function

$$\Psi(x,t) = \boldsymbol{C}^{\mathrm{T}}(t)\boldsymbol{\psi}(x). \tag{18}$$

In Eq. (18), $\boldsymbol{C}(t)$ is the vector with l_{max} components determined from (17), and $\boldsymbol{\psi}(x) = (\psi_1(x), \ldots, \psi_{s_{max}}(x))^{\mathrm{T}}$. The Hamiltonian in (17) is time-periodic, i.e., $H(x,t) = H(x, t + NT)$ for any integer N, where the period $T = 2\pi/\omega$. The frequency ω of the driving field is tuned to match the splitting of the Zeeman doublet of the discrete state, $\hbar\omega = E_2 - E_1$. Since the driving is periodic, we can apply the Floquet technique [13,36–39] to obtain the stroboscopic picture of the

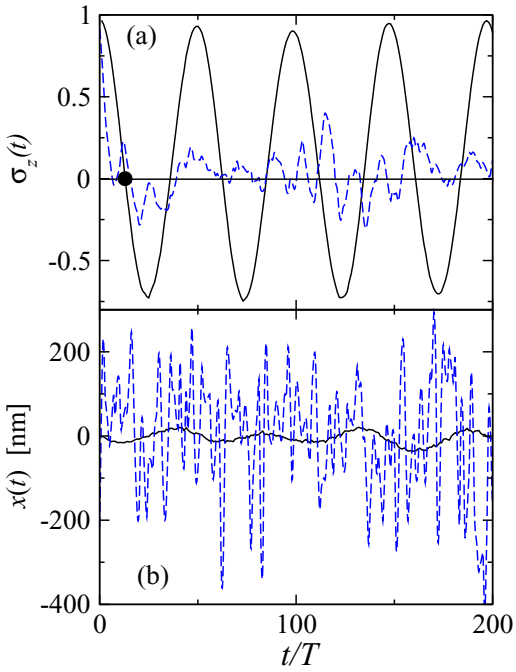

FIG. 2. Stroboscopic dynamics for mean values of (a) spin component $\sigma_z(t)$ and (b) coordinate $x(t)$ for parameters $B = 0.5B_m$ and $\alpha = 6$ meV nm. The amplitude of the driving electric field $F_0 = 0.5$ V/cm (solid line) and $F_0 = 1.5$ V/cm (dashed line). The black circle in (a) corresponds to $T_{sf}/2$ for $F_0 = 0.5$ V/cm.

system state $\Psi(x,t)$ at discrete moments of time $t = NT$ [39,40].

When the wave function (18) is found, one can calculate the stroboscopic evolution of various observables such as

$$x(t) = \int_{-\infty}^{\infty} \Psi^{\dagger}(x,t)x\Psi(x,t)dx \tag{19}$$

for the position and

$$\sigma_z(t) = \int_{-\infty}^{\infty} \Psi^{\dagger}(x,t)\sigma_z\Psi(x,t)dx \tag{20}$$

for the spin component. We take the initial state $\Psi(x,0)$ as the ground state E_1, which has a spin component $\sigma_z(0)$ close to 1. When the first zero of $\sigma_z(t) = 0$ is achieved [as shown in Fig. 2(a)] during the stroboscopic evolution, we define this time as half of the "spin-flip" time T_{sf}. For a few certain values of the system parameters and driving fields, it is possible that the condition $\sigma_z(t) = 0$ is never reached throughout the observation interval. In such a case, we define the spin-flip rate $1/T_{sf}$ as equal to zero.

B. Numerical results

1. System parameters

We begin by setting the parameters for numerical calculations. We use a donor state in InSb quantum wire. For InSb the value $m = 0.0136m_0$ is chosen for the electron effective mass where m_0 is the mass of a free electron [41]. We assume $g = -50.6$ for the electron g-factor in InSb. The amplitude of the Rashba SOC α in InSb can be tuned by the gate voltage and can reach high values up to 100 meV nm [42,43].

For the shallow donor parameters, we accept $U_0 = 1.5$ meV and $d = 10$ nm, as can be realized for a donor screened by a two-dimensional electron gas [44]. As a result, a single discrete level $E_0 = -0.072$ meV, corresponding to the localization length l close to 200 nm and frequency $|E_0|/\hbar \approx 2\pi \times 17.8$ GHz, is formed. All the states with positive energies belong to the continuum. For the chosen parameters, Eq. (5) gives the value $B_m = 25$ mT. We consider three values of magnetic field: $B = 0.25B_m$, $0.5B_m$, and $0.75B_m$, and for each B we take two values of SOC: $\alpha = 6$ meV nm (for relatively weak SOC with $l_{so} = \hbar^2/m\alpha \approx 10^3$ nm $> l$) and $\alpha = 25$ meV nm (for relatively strong SOC where $l_{so} \approx l$). The basis in Eq. (18), truncated at $s_{max} = 250, \ldots, 500$, provides a good, s_{max}-independent, convergence of all the numerical results in the range where the continuum states are effectively involved in the evolution by the electric fields.

The condition of strong driving field amplitude $F_s \sim |E_0/le|$ in Eq. (4) yields ~ 5 V/cm. Although this value is experimentally accessible, we will limit our calculations to lower fields to avoid a nonlinear ionization process that is far beyond Fermi's golden rule [45]. Indeed, the semiclassical tunneling probability for a static field F_0 per time $\hbar/|E_0|$ can be estimated as $\exp(-4F_s/3F_0)$, and one can introduce as a nominal reference parameter the tunneling ionization time $\tau_{ti} = \hbar/|E_0| \times \exp(4F_s/3F_0)$. Since the electric fields of our interest during the oscillation period are considerably weaker than F_s, the system is stable against the ionization at a sufficiently long time scale.

2. Time dependence of observables

To demonstrate a typical time dependence of the observables of interest, we show in Fig. 2 two examples of the evolution for mean values $\sigma_z(NT)$ and $x(NT)$ for driving fields with $F_0 = 0.5$ and 1.5 V/cm, on the time interval $N < 200$ of the driving field periods. Other parameters are $B = 0.5B_m$ and $\alpha = 6$ meV nm giving the level splitting $E_2 - E_1 = 0.035$ meV equal to $\approx 2\pi \times 8.65$ GHz of the driving frequency. It should be mentioned that this splitting includes the Zeeman coupling and the contribution due to the presence of the continuum states, which, at weak SOC, is proportional to the square of the Rashba SOC strength [see Eq. (15)]. In experiment, the driving frequency can be tuned smoothly to match the exact level splitting, which may differ from the simple Zeeman term. Note that this frequency, being a reference parameter, and independent of the driving field, does not include the dynamical Stark effect [46].

It can be seen that at low driving amplitude, the dynamics of both spin and coordinate mean values shown in Fig. 2 is rather regular, especially for the spin, where it is reminiscent of the well-known picture for the Rabi resonance in a two-level system with the frequency close to $e|x_{\lambda\lambda'}|F_0/\hbar$. As to the coordinate mean value, it demonstrates the combined drift and oscillations, which do not exceed the localization length, being of the order of 40–80 nm. Thus, for low amplitudes of driving the influence of delocalized continuum states of the nanowire is relatively small both for spin and coordinate dynamics as it can be reduced mostly to the formation of

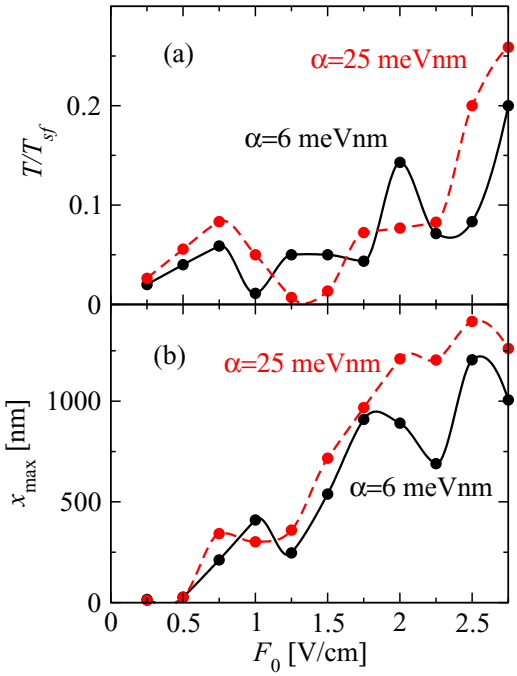

FIG. 3. Electric field amplitude dependence of (a) the spin-flip rate $1/T_{\rm sf}$ and (b) the maximum displacement $x_{\rm max}$ for different parameters of the spin-orbit coupling strength α and for $B = 0.5B_{\rm m}$: $\alpha = 6$ meV nm (solid lines) and $\alpha = 25$ meV nm (dashed lines). The lines serve only as guides for the eye.

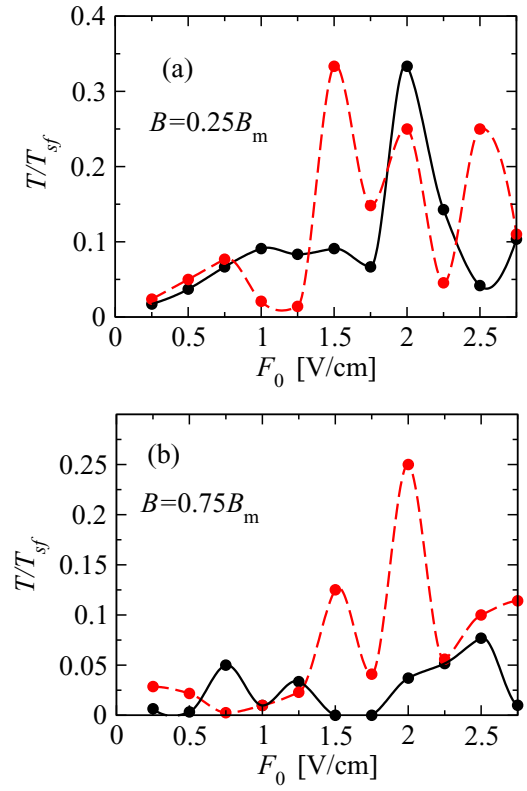

FIG. 4. (a) Spin-flip rate for magnetic field $B = 0.25B_{\rm m}$. The parameters of the spin-orbit coupling strength are $\alpha = 6$ meV nm (solid line) and $\alpha = 25$ meV nm (dashed line). (b) Same as in (a) but for higher magnetic field $B = 0.75B_{\rm m}$. The lines serve only as guides for the eye.

a nonzero matrix element of a coordinate between localized spin-up and spin-down states.

The situation changes when the driving amplitude is increased to $F_0 = 1.5$ V/cm. It can be seen that both the spin and the coordinate lose their simple evolution pattern visible at low driving field. They now demonstrate more complicated dynamics with obviously many states participating in it. This result clearly reflects the presence of continuum states in the driven evolution, which become more significant when the driving amplitude is increased. As to the numerical values in Fig. 2, one can see that the spin projection $\sigma_z(t)$ never approaches -1, i.e., no full spin flip is achieved. We attribute this effect to the presence of many states with different spin projections and with comparable weights in the total wave function (18). The coordinate mean value $x(t)$ at strong driving also demonstrates a complicated and irregularly oscillating behavior, with much greater amplitude than for weak driving, approaching or even exceeding the localization length l. This can be described as more evidence of the significant contribution of continuum states in the driven dynamics, even for moderate fields less than 3 V/cm.

3. Dependence on the driving field amplitude

It is of interest to track the amplitude characteristics of spin resonance as functions of the driving field amplitude. First of all, we consider the dependence of the spin-flip rate $1/T_{\rm sf}$ in units of $1/T$, and we find it for several values of the field amplitude F_0 as plotted in Fig. 3. Two values of the SOC coupling constant are taken for the magnetic field $B = 0.5B_{\rm m}$. One can see that for both SOC amplitudes even at a moderate driving field amplitude $F_0 \approx 0.75$ V/cm, the dependence of $1/T_{\rm sf}$ on F_0 becomes strongly nonlinear due to the significant role of continuum states in the driven dynamics, taking the system out of a simple two-level approximation. A similar behavior of the spin-flip frequency in a multilevel system has been observed in our previous studies of the spin resonance in a double quantum dot [37]. The complicated behavior of coupled spin and charge observables was also observed in a multilevel system represented by a driven two-dimensional quantum billiard with SOC [38]. One can see in Fig. 3 as well as in Fig. 4 that for certain values of the driving field, the spin-flip rate decreases to zero. The definition of such a case has been discussed at the end of Sec. IV A, and it represents rare cases in which the condition $\sigma_z(t) = 0$ is never reached during the observation time. The main cause of this effect cannot be assigned to the dynamical shift of the resonance condition [45,46] since the significant presence of the continuum states with variable spin projections produces a much more complex coupled spin-position dynamics than that solely caused by a time-dependent Stark effect. This is supported by an observation that the regions with zero $1/T_{\rm sf}$ occupy only a few intermediate points for driving field amplitudes F_0 in Figs. 3 and 4. One can see there that an increase in F_0 generates no results with vanishing $1/T_{\rm sf}$ for F_0 close to the maximum values, so the observed feature is not definitely related to the dynamic energy level shift, which grows with the increasing driving field.

Another characteristic of the driven evolution is the maximum achievable displacement during the total observation time, $x_{\max}$, shown in Fig. 3(b) for the same other parameters as in Fig. 3(a). One may expect that the absolute value $x_{\max}$ grows monotonically upon increasing the electric-field strength F_0. However, strong SOC and the presence of the continuum provide sizable corrections to such a simple estimate, as can be seen in Fig. 3. First of all, the dependence of $x_{\max}$ on F_0 demonstrates a nonlinear character from the fields of about 1 V/cm for $\alpha = 6$ meV nm and from 0.75 V/cm for $\alpha = 25$ meV nm. For the field amplitude exceeding $F_0 \approx 1.5$ V/cm, a saturation tendency is clearly visible, indicating that the electric-field efficiency in displacing the electron at large distance is strongly reduced.

One can be interested to look at the characteristics of the spin resonance also for other values of the external magnetic field. Here we show the results for the spin-flip rate for the field $B = 0.25B_{\mathrm{m}}$ in Fig. 4(a) and for $B = 0.75B_{\mathrm{m}}$ in Fig. 4(b). As in Fig. 3, for each field we consider two values of the SOC amplitude $\alpha = 6$ and 25 meV nm.

By analyzing the results in Figs. 3 and 4, one can conclude that both spin and coordinate dynamics have a lot of common features for different parameters of the magnetic field and SOC. The nonlinear dependence of the spin-flip rate $1/T_{\mathrm{sf}}$ and the maximum mean value of the electron displacement $x_{\max}$ on the driving field amplitude are clearly visible. The maximum values of $1/T_{\mathrm{sf}}$ are comparable for all magnetic fields and for all SOC amplitudes. However, it can be seen from Fig. 4(b) that the increase in the magnetic field to $0.75B_{\mathrm{m}}$ reduces the SOC-induced coupling between the states with different spin. Indeed, for this field, the values of $1/T_{\mathrm{sf}}$ are in general lower than those for $B = 0.25B_{\mathrm{m}}$ and $0.5B_{\mathrm{m}}$. This finding is especially clear for the low SOC strength $\alpha = 6$ meV nm. As one can see in all the figures, the spin-flip time T_{sf} usually does not exceed the nominal tunneling ionization time τ_{ti}, (defined in the last paragraph of Sec. IV B 1) confirming that the time scale of the spin-flip process is usually shorter than the time scale of the tunneling ionization [40].

The two values of Rashba coupling considered here represent its actual operating range in prospective systems based on InSb nanowires. Indeed, neither very small nor very large SOC is desirable. If the SOC is too weak, the coupling between spin-resolved discrete states via the continuum becomes ineffective. For a very strong coupling one needs large amplitudes F_0 to flip the spin and to make the qubit actually work since highly mixed spin states are involved and produced by the driving. As a result, a certain range of the SOC strength is needed, as represented by these two realizations.

Another key parameter is the driving field amplitude F_0, limited here by a moderate value of 2.75 V/cm. The first reason for keeping it not very strong is to avoid the nonlinear ionization [45]. The second reason is the absence of an effective increase for the spin-flip rate when making the driving amplitude too strong, as can be seen in Figs. 3 and 4. When the driving is too intense, the continuum states with different spins begin to play a more significant role by creating a hardly distinguishable mixture of the two discrete states with the continuum. In such a mixture, the spin components together with the wave-function spread may become poorly defined, prohibiting the application of such a regime for a practically operating qubit. Besides, strong electric fields are in general not desirable for micron- and submicron-sized electronic devices. This is why we restrict ourselves to low and medium driving fields, sufficient for providing an effective operation for the qubit.

Here one additional comment might be of interest. Although the behavior of the driven spin dynamics in the regime of strong spin-orbit coupling is practically unpredictable, some conclusions can be made from the extension of the perturbation theory analysis. In this case, the matrix element of the coordinate $x_{\lambda\lambda'}$ is of the order of the localization length l. Therefore, the spin-flip Rabi frequency of the order of $eF_0 l/\hbar$ sets the upper limit on the spin-flip rate for a relatively weak external field, which is confirmed by our results in Fig. 2 for lower amplitude F_0. For a strong field and a relatively weak spin-orbit coupling, we can conclude from the matrix element on Eq. (13) that the states providing the maximal contribution to (13) and to the spin dynamics have momenta of the order of $\hbar/l$. Therefore, they are described by the precession rate of the order of $\alpha/\hbar l$, which may help to estimate the actual spin-flip rate. However, it can be seen in Figs. 3 and 4 that an increase in the SOC amplitude alone does not lead to the strictly proportional growth of the spin-flip rate since the dynamics has a complex nature with many states participating in it.

We note that in all the regimes considered here, T_{sf} is of the order of or less than $10T$. Taking into account that T is of the order of 0.1 ns, we find that T_{sf} is of the order of a nanosecond. Since the spin relaxation time in weak magnetic fields exceeds this time by orders of magnitude [34,47], at a time scale of $N \sim 100$, we still have a coherent qubit manipulation in the EDSR regime. Note that the effect of noise on the electric field that is always present in the semiconductor system of interest will not change this result since the spectrum of the noise is not peaked in the frequency range corresponding to the EDSR in the magnetic fields considered in this paper [48].

V. CONCLUSIONS

We studied the electric dipole spin resonance for a nanowire-based donor state coupled to the continuum, the latter playing a critical role in the dynamics. The continuum leads to a strongly nonlinear dependence of the coupled evolution of spin and position on the electric field. Qualitative features of this nonlinear behavior are presented by strong differences of the system dynamics from conventional Rabi-like oscillations, including incomplete spin flips.

The observed characteristics of both spin and position dynamics, having much in common, for different values of magnetic field and spin-orbit coupling can be of interest for designing novel types of spin and charge qubits when the confining potentials are shallow, and the discrete states strongly interact with the continuum during the qubit operation. For this reason, these effects should be taken into account for possible applications of materials with strong spin-orbit coupling, such as InSb, for fabricating qubit-processing structures.

ACKNOWLEDGMENTS

D.V.K. and E.A.L. are supported by the State Assignment of the Ministry of Education and Science RF (Project

No. 3.3026.2017/PCh). E.A.L. was supported by the Grant of the President of the Russian Federation for young scientists MK-6679.2018.2. E.Y.S. acknowledges support by the Spanish Ministry of Economy, Industry and Competitiveness (MINECO) and the European Regional Development Fund FEDER through Grant No. FIS2015-67161-P (MINECO/FEDER, UE), and the Basque Government through Grant No. IT986-16.

[1] E. I. Rashba, Sov. Phys. Solid State **2**, 1109 (1960).
[2] G. Bemski, Phys. Rev. Lett. **4**, 62 (1960).
[3] R. L. Bell, Phys. Rev. Lett. **9**, 52 (1962).
[4] Y. A. Bratashevskii, A. A. Galkin, and Y. M. Ivanchenko, Sov. Phys. Solid State **5**, 260 (1963).
[5] E. I. Rashba and V. I. Sheka, Sov. Phys. Solid State **6**, 114 (1964).
[6] E. I. Rashba and V. I. Sheka, Sov. Phys. Solid State **6**, 451 (1964).
[7] E. I. Rashba and Al. L. Efros, Phys. Rev. Lett. **91**, 126405 (2003).
[8] J. Ibañez-Azpiroz, A. Eiguren, E. Ya. Sherman, and A. Bergara, Phys. Rev. Lett. **109**, 156401 (2012); J. Ibañez-Azpiroz, A. Bergara, E. Ya. Sherman, and A. Eiguren, Phys. Rev. B **88**, 125404 (2013).
[9] A. F. Sadreev and E. Ya. Sherman, Phys. Rev. B **88**, 115302 (2013).
[10] K. C. Nowack, F. H. L. Koppens, Yu. V. Nazarov, and L. M. K. Vandersypen, Science **318**, 1430 (2007).
[11] X. Hu, Y.-X. Liu, and F. Nori, Phys. Rev. B **86**, 035314 (2012).
[12] V. N. Golovach, M. Borhani, and D. Loss, Phys. Rev. B **74**, 165319 (2006).
[13] J. H. Jiang, M. Q. Weng, and M. W. Wu, J. Appl. Phys. **100**, 063709 (2006).
[14] M. Borhani and X. Hu, Phys. Rev. B **85**, 125132 (2012).
[15] M. P. Nowak, B. Szafran, and F. M. Peeters, Phys. Rev. B **86**, 125428 (2012).
[16] J. Romhányi, G. Burkard, and A. Pályi, Phys. Rev. B **92**, 054422 (2015).
[17] Y. Ban, X. Chen, E. Ya. Sherman, and J. G. Muga, Phys. Rev. Lett. **109**, 206602 (2012).
[18] M. T. Veszeli and A. Pályi, Phys. Rev. B **97**, 235433 (2018).
[19] R. Li, J. Q. You, C. P. Sun, and F. Nori, Phys. Rev. Lett. **111**, 086805 (2013); R. Li and J. Q. You, Phys. Rev. B **90**, 035303 (2014).
[20] S. Nadj-Perge, S. M. Frolov, E. P. A. M. Bakkers, and L. P. Kouwenhoven, Nature (London) **468**, 1084 (2010).
[21] E. N. Osika and B. Szafran, J. Phys.: Condens. Matter **27**, 435301 (2015).
[22] Y. Oreg, G. Refael, and F. von Oppen, Phys. Rev. Lett. **105**, 177002 (2010).
[23] A. Das, Y. Ronen, Y. Most, Y. Oreg, M. Heiblum, and H. Shtrikman, Nat. Phys. **8**, 887 (2012).
[24] P. W. Brouwer, M. Duckheim, A. Romito, and F. von Oppen, Phys. Rev. Lett. **107**, 196804 (2011).
[25] W. DeGottardi, D. Sen, and S. Vishveshwara, Phys. Rev. Lett. **110**, 146404 (2013).
[26] I. Adagideli, M. Wimmer, and A. Teker, Phys. Rev. B **89**, 144506 (2014).
[27] A. Pitanti, D. Ercolani, L. Sorba, S. Roddaro, F. Beltram, L. Nasi, G. Salviati, and A. Tredicucci, Phys. Rev. X **1**, 011006 (2011).
[28] X. Linpeng, T. Karin, M. V. Durnev, R. Barbour, M. M. Glazov, E. Y. Sherman, S. P. Watkins, S. Seto, and K.-M. C. Fu, Phys. Rev. B **94**, 125401 (2016); X. Linpeng, M. L. K. Viitaniemi, A. Vishnuradhan, Y. Kozuka, C. Johnson, M. Kawasaki, and K.-M. C. Fu, Phys. Rev. Appl. **10**, 064061 (2018).
[29] L. D. Landau and E. M. Lifshitz, *Quantum Mechanics—Nonrelativistic Theory*, 3rd ed., Course of Theoretical Physics Vol. 3 (Elsevier, Amsterdam, 1977).
[30] F. Mireles and G. Kirczenow, Phys. Rev. B **64**, 024426 (2001).
[31] M. M. Gelabert, L. Serra, D. Sánchez, and R. López, Phys. Rev. B **81**, 165317 (2010).
[32] A. N. M. Zainuddin, S. Hong, L. Siddiqui, S. Srinivasan, and S. Datta, Phys. Rev. B **84**, 165306 (2011).
[33] L. Xu, X.-Q. Li, and Q.-F. Sun, Sci. Rep. **4**, 7527 (2014).
[34] A. V. Khaetskii and Yu. V. Nazarov, Phys. Rev. B **64**, 125316 (2001).
[35] One can estimate the number of continuum states $\mathcal{N}$ occupying the typical energy interval of the order of $|E_0|$ as $\mathcal{N} \sim L/l \gg 1$. This inequality assures a large density of the extended states and represents a validity approximation for the continuum. In our numerical studies, we took $\mathcal{N} \approx 10^2$, which gave us a reliable approach for the continuum states.
[36] L. E. Reichl, *The Transition to Chaos. Conservative Classical Systems and Quantum Manifestations*, 2nd ed. (Springer-Verlag, New York, 2004).
[37] D. V. Khomitsky, L. V. Gulyaev, and E. Ya. Sherman, Phys. Rev. B **85**, 125312 (2012).
[38] D. V. Khomitsky, A. I. Malyshev, E. Ya. Sherman, and M. Di Ventra, Phys. Rev. B **88**, 195407 (2013).
[39] V. Ya. Demikhovskii, F. M. Izrailev, and A. I. Malyshev, Phys. Rev. E **66**, 036211 (2002); Phys. Rev. Lett. **88**, 154101 (2002).
[40] See Supplemental Material at http://link.aps.org/supplemental/10.1103/PhysRevB.99.014308 for details of the stroboscopic approach and short-time dynamics, including the effects of tunneling.
[41] I. Saïdi, S. Ben Radhia, and K. Boujdaria, J. Appl. Phys. **107**, 043701 (2010).
[42] M. A. Leontiadou, K. L. Litvinenko, A. L. Gilbertson, C. R. Pidgeon, W. R. Branford, L. F. Cohen, M. Fearn, T. Ashley, M. T. Emeny, B. N. Murdin, and S. K. Clowes, J. Phys.: Condens. Matter **23**, 035801 (2011).
[43] P. Wójcik, A. Bertoni, and G. Goldoni, Phys. Rev. B **97**, 165401 (2018).
[44] T. Ando, A. B. Fowler, and F. Stern, Rev. Mod. Phys. **54**, 437 (1982).
[45] N. B. Delone and V. P. Krainov, *Atoms in Strong Light Fields*, Springer Series in Chemical Physics (Springer, Heidelberg, 1985).
[46] In the absence of SOC, in a weak static electric field F both spin-split localized states experience a Stark shift $E_0(F/F_s)^2$, as can be found from perturbation theory using Eq. (13). Their second-order in α Stark-originated splitting is then of the order

of $E_0(F/F_s)^2 \times (l/l_{so})^2$. As a result, for the set of magnetic fields of our interest, the direct effect of the relative Stark shift compared to the effective Zeeman splitting becomes important if both the driving field and the spin-orbit coupling are relatively strong.

[47] S. Amasha, K. MacLean, I. P. Radu, D. M. Zumbühl, M. A. Kastner, M. P. Hanson, and A. C. Gossard, Phys. Rev. Lett. **100**, 046803 (2008).

[48] A discussion of frequency-dependent noise can be found in R. Li, J. Phys.: Condens. Matter **30**, 395304 (2018).